

Observation of Magnetic Supercooling of the Transition to the Vortex State

J.P. Davis¹, D. Vick², J.A.J. Burgess^{1,2}, D.C. Fortin¹, P.

Li², V. Sauer^{1,2}, W.K. Hiebert² and M.R. Freeman^{1,2}

¹ *Department of Physics, University of Alberta,*

Edmonton, Alberta, Canada T6G 2G7 and

² *National Institute for Nanotechnology,*

Edmonton, Alberta, Canada T6G 2M9

(Dated: Version August 27, 2022)

Abstract

We demonstrate that the transition from the high-field state to the vortex state in a nanomagnetic disk shows the magnetic equivalent of supercooling. This is evidence that this magnetic transition can be described in terms of a modified Landau first-order phase transition. To accomplish this we have measured the bulk magnetization of single magnetic disks using nanomechanical torsional resonator torque magnetometry. This allows observation of single vortex creation events without averaging over an array of disks or over multiple runs.

PACS numbers: 75.70.Kw, 75.60.-d, 75.40.-s, 85.85.+j

The Landau-Lifshitz-Gilbert (LLG) equation for the time evolution of magnetic texture has been extremely successful in describing the fast (sub-picosecond to nanosecond) magnetization dynamics in nanomagnetic elements [1]. On the opposite extreme, the static ground state of nanomagnetic elements can be solved analytically [2, 3]. The desire to explore magnetism outside these regimes has lead researchers to pursue ultra-fast (femtosecond) magnetic switching, for example, by optical polarization analysis [4], electrical spin currents [5], or other techniques [6, 7]. There are also magnetic phenomenon that occur outside the scope of these descriptions on intermediate times scales (seconds to minutes), called magnetic after effects (MAE) or magnetic viscosity [8–10], when an existing magnetic structure, like a domain wall, undergoes thermal diffusion. In this Letter, we present nanomechanical torque magnetometry measurements of a single nanomagnetic disk, which reveal another magnetic phenomenon that occurs on intermediate time scales, that is, the magnetic equivalent of supercooling. In a micro/nano magnetic disk, it has been predicted that vortex creation can be described by a modified Landau first-order phase transition [11], with a corresponding supercooling of the high-field to vortex-state transition. Unlike a MAE this does not occur from thermal diffusion of an existing vortex, but instead from a barrier to nucleation of the vortex. This is consistent with our observations.

In a micro/nano magnetic disk with a large diameter-to-thickness ratio in zero applied magnetic field the ground state is that of a magnetic vortex [2, 3, 12]. The magnetization curls in the plane of the disk and there is a vortex core associated with the singularity of curling magnetization, where the magnetization points out of the plane of the disk. At large applied in-plane magnetic fields, the disk’s energy is minimized by the parallel-spin state, in which the magnetization is aligned with the applied field. At intermediate fields another magnetic state, the C-state, exists which can be thought of as a buckled form of the parallel-spin state. The magnetization curls in the plane of the disk and a virtual vortex core lies outside of the disk [13]. Other buckled states exist such as the S-state and onion state, but for simplicity we limit the discussion to the C-state.

In the theory of Ref. [11], vortex creation is described by a modified Landau first-order phase transition, where the applied field plays the role typically reserved for temperature [14] and there is a critical magnetic field, H_c , instead of a critical temperature. H_c is the highest magnetic field that produces vortex creation. The order parameter associated with this phase transition is $\psi = s^{-1}$, where s is the normalized distance between the center of the disk and the ‘rigid’ vortex core [11]. ψ is zero in the parallel-spin state, describes a continuous transition to the C-state and a discontinuous transition to the vortex state. The free energy of the system can be expanded in even

powers of ψ and the transition from the parallel-spin state to the C-state is second-order, whereas the transition from either the parallel-spin state or the C-state to the vortex state is first-order. The broken symmetry associated with the first-order phase transition is the out-of-plane magnetization of the vortex core.

A signature of a first-order phase transition is supercooling, associated with the nucleation of one state from the other [15]. The amount of supercooling is dependent on the intrinsic energy barrier to nucleation, and extrinsic factors such as the surface roughness [16] and the rate at which the temperature (here magnetic field) is lowered. Experimental tests of this phase transition theory have not been undertaken, until now, because typical experiments on nanoscale magnetic elements involve averages over arrays of elements or averages over many runs.

Our measurement is based on torque magnetometry, in which a magnetic element with magnetization \mathbf{M} , in the presence of an applied magnetic field, \mathbf{H} , experiences a torque, $\boldsymbol{\tau} = \mathbf{M} \times \mathbf{H}$. In our geometry, we are sensitive to the magnetization in the \hat{x} direction, the torquing magnetic field is in \hat{z} (out of the plane) and the torsion rod is oriented along \hat{y} , Fig. 1c. The torque is detected as an out-of-plane displacement of the torsion paddle [17]. We apply a constant AC magnetic field, H_z , at the resonance frequency of the torsional resonator. The primary torsional mode, as shown in Fig. 1d, is at 2.81 MHz and has a mechanical Q of 500. We detect an optical interferometric signal through one of the large paddles at the resonant frequency, which is proportional to the out-

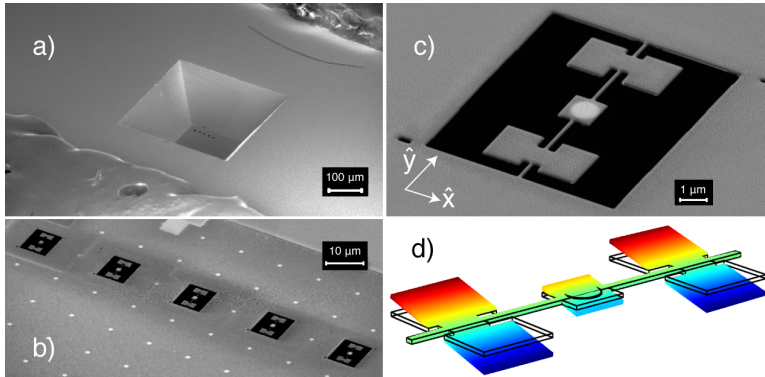


FIG. 1: Color online. SEM micrographs of (a) the silicon nitride membrane on the silicon frame, (b) the array of magnetic disks visible through the silicon nitride with the nano-torsional resonators fabricated around the disks (just barely observable in a), and (c) the resonator used in this Letter (also the lower right resonator in b). (d) Finite element model of the primary torsional mode, in which all three paddles oscillate in phase.

of-plane displacement. This is sensitive ($6 \times 10^7 \mu_B$) to changes in the magnetization, M_x , of the magnetic element on the torsional resonator, which is varied by controlling the applied magnetic field along \hat{x} , H_x . Further details can be found elsewhere [17].

Device fabrication starts with a low-stress silicon nitride membrane on a silicon frame [18], Fig. 1a. We deposit 42 ± 2 nm thick, as measured by calibrated atomic force microscopy, permalloy disks via collimated electron beam deposition at 10^{-9} mbar on the nitride using a stencil mask [19] with $1 \mu\text{m}$ diameter holes and $12 \mu\text{m}$ spacing. A 2 nm gold anti-charging layer is sputtered onto the opposite side of the nitride membrane. The frame is mounted, magnetic element side down, as in Fig. 1a. The magnetic disks are visible through the silicon nitride with a scanning electron microscope, aligned to be coincident with a focused-ion-beam mill. This allows fabrication of a torsional resonator around a magnetic disk, Figs. 1b-c. The resonator shown in Fig. 1c is used for all measurements in this Letter. The device is mounted $31 \mu\text{m}$ from a silicon wafer, which acts as the back mirror of a low finesse Fabry-Perot cavity, and the entire structure is mounted on a 2D Hall probe (H_x, H_y) in a vacuum chamber [17]. All measurements were performed at room temperature and the laser (HeNe, 632.8 nm, $3 \mu\text{W}$ hitting the resonator) for optical detection was kept at constant power for all measurements.

There are two applied magnetic fields in the experiment. The first is the AC magnetic field at 2.81 MHz along \hat{z} . Increasing this field increases the amplitude of the detected interferometric signal, but has no effect on the statistics of vortex creation and annihilation for our accessible field range. Nonetheless, it is kept constant in all measurements (0.81 kA/m peak-to-peak). The second magnetic field is the bias field which is applied along \hat{x} and varies M_x in the disk. Sweeps of H_x are shown in Fig. 2. At large bias fields M_x is saturated in the parallel-spin state. This has been confirmed by micromagnetic simulations and is shown as the red disk in Fig. 2, although it can be seen that this is not a perfect parallel-spin state. As the bias field is lowered there is a jump upwards then a small plateau, which we do not understand at this time. This is followed by a downward kink and then a sharp drop as the magnetic vortex enters the disk and the magnetization drops abruptly. The kink is associated with the buckling of the parallel-spin state [20]. The disk is relatively large at $1 \mu\text{m}$ diameter so it is difficult to state with certainty that this is the parallel-spin to C-state transition. At zero field the vortex sits near the center of the disk, which has been confirmed by Lorentz microscopy [21] and micromagnetic simulations, shown as insets to Fig. 2. As the applied field is increased from zero the vortex is displaced from the center of the disk and is eventually annihilated, which corresponds to a smaller, but also abrupt change in M_x [2, 3]. All

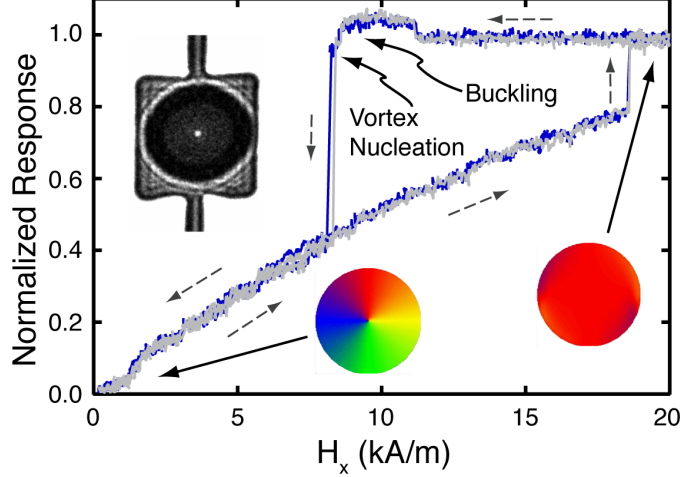


FIG. 2: Color online. Interferometric response at 2.81 MHz versus applied bias magnetic field, H_x . There are two hysteresis loops, measured starting at saturation and following the dashed arrows, with different creation fields but identical annihilation fields. Inset is a Lorentz micrograph [21] of the disk on the central paddle of the resonator. The white spot in the center of the disk originates from the chirality of the vortex state. We also show micromagnetic simulations of the in-plane magnetization. The color map is: red is \hat{x} , blue is $-\hat{y}$, green is $-\hat{x}$, yellow is \hat{y} .

of these features can be seen in Fig. 2. The vortex creation and annihilation events occur over a small magnetic field, ~ 0.02 kA/m. Experimental techniques that measure arrays of elements or average over multiple events would observe broadened transitions.

Fig. 2 displays two individual hysteresis sweeps with their corresponding vortex creation and annihilation fields. Repeated measurements of the events can be performed to learn about the statistics governing them. In Fig. 3 we show a series of histograms showing the applied fields at which the vortex creation and annihilation events occur. Figs. 3a and 3e correspond to low sweep rates, Figs. 3b and 3f to intermediate sweep rates, and Figs. 3c and 3g to high sweep rates. The sweep rate is field dependent, since we sweep the position of a permanent magnet at a constant rate.

We observe that the vortex creation and annihilation field distributions are bimodal. If during a field sweep down a vortex is created below 7 kA/m, then that same vortex annihilates during the subsequent field sweep up at a lower bias field than any vortex created above 7 kA/m. This phenomenon is not sweep rate dependent and is not the focus of this manuscript. It will be explored elsewhere. Instead we focus on the $92 \pm 4\%$ of events that correspond to vortex creation above 7

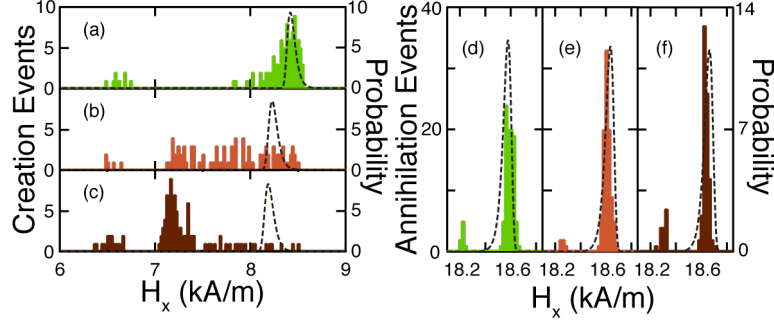


FIG. 3: Color online. Histograms (left axis) of the magnetic fields of vortex creation and annihilation events binned by 0.02 kA/m. Each panel has the same area and 100 events. The dashed curve (right axis) is the probability distributions predicted by a thermally driven process over a field dependent energy barrier [22], see text. (a) Vortex creation at a sweep rate of 0.02 kA/m·s, (b) 0.14 kA/m·s, and (c) 0.36 kA/m·s. (d) Vortex annihilation at 0.07 kA/m·s, (e) 0.43 kA/m·s, and (f) 1.16 kA/m·s. The probability distributions match reasonably well to the bias fields, widths and sweep rate dependence for vortex annihilation, but do not for vortex creation.

kA/m and the main annihilation peak.

Vortex creation occurs over a broader range of fields than vortex annihilation. In the first-order phase transition model this spread in vortex creation fields is natural: the vortex is energetically favored to be inside the magnetic disk at the highest field at which creation occurs (8.5 kA/m), but there is a barrier to nucleating the vortex core with out-of-plane magnetization. This leads to supercooling of the high-field state and the spread of vortex creation fields.

Figs. 3a-c show that vortex creation occurs at lower bias fields for faster bias field sweep rates. This rate dependence demonstrates that vortex nucleation occurs on laboratory time scales (the dynamics associated with the magnetization changes occur on picosecond time scales, but the vortex nucleation itself requires much longer waits). The kink in Fig. 2 that we associate with the buckling transition from parallel-spin state to the C-state [20] always occurs at 8.55 ± 0.06 kA/m; it does not show supercooling or sweep rate dependence. This is as expected from the theory of Ref. [11], in which this transition is of second-order and should not demonstrate supercooling, although confirmation of the second-order nature of the transition will require improvements in signal-to-noise. In Fig. 4a, we plot the mean vortex creation field as a function of sweep rate. The sweep rate dependence is a classic effect in supercooled first-order phase transitions [15, 16]. Figs. 3e-g reveal that there is also a small amount of rate dependence to the vortex annihilation

field distribution, which we plot in Fig. 4b. The rate dependence of vortex creation is more than an order of magnitude larger than vortex annihilation.

We compare our data with an Arrhenius relation for the probability per unit time of nucleating or annihilating a vortex, $dN/dt = f_0 e^{-E(H)/k_B T}$ [9, 10] with a field dependent energy barrier [22] and thermal activation over the barrier. f_0 is an attempt frequency given by the order of magnitude of the frequency of spin waves at edge of the magnetic disk [23], 10^9 Hz for vortex nucleation, and by the gyrotropic frequency for annihilation, 10^8 Hz [24]. $E(H)$ is the energy associated with the magnetic volume, V , involved in the switching event, given by $E = (1 - H/H_a)^{3/2} \mu_0 M_s^2 V/2$ for annihilation and $E = (H/H_n - 1)^{3/2} \mu_0 M_s^2 V/2$ for creation [22]. M_s is the saturation magnetization for permalloy (800 kA/m) and μ_0 is $4\pi \times 10^{-7}$ N/A². There are three parameters in the model: f_0 , V , and either H_n or H_a for nucleation or annihilation respectively. We fix f_0 to be the values above (the fit is not very sensitive to f_0) and vary V and H_n (H_a) to match the bias field, width, and sweep rate dependence of the distributions.

Probability distributions calculated from this model are shown in Figs. 3d and 3h. Vortex annihilation is well modeled with $H_a = 19.5$ kA/m and a volume corresponding to a cylinder of 12.3 nm radius and 42 nm height. This is a slightly larger than expected, but reasonable, volume involved in the annihilation [2, 25]. Our best fit the creation data is shown in Fig. 3d, with $H_n = 7$ kA/m and a cylinder of 4.5 nm radius and 42 nm height. We note that in many thousands of runs we have never observed a vortex creation event above 8.5 kA/m. This, along with the fact an H_n greater than 7 kA/m is unphysical, place additional constraints on the fit parameters. Fig. 3d shows that the thermal nucleation model does not capture the physics of vortex creation and we suggest that the critical field is instead 8.5 kA/m with corresponding supercooling. The fundamental difference between vortex nucleation and annihilation is that there is broken symmetry, the formation of an out of plane magnetization, that must occur to form the vortex state.

Rotation of the applied bias field by small angles, θ , shown in Fig. 4c, changes the location of vortex creation and annihilation along the magnetic disk's perimeter. This affects the amount of supercooling possible at a given temperature and sweep rate, due to the effective magnetic roughness of the disk's edge. In Fig. 4d, we show two histograms. The purple histogram shows significant supercooling and corresponds to 0 degrees, the same angle as all measurements discussed above. The orange histogram is for the bias field rotated by 2 degrees. The supercooling effect is entirely removed and the vortex creation becomes narrowly peaked, even at fast sweep

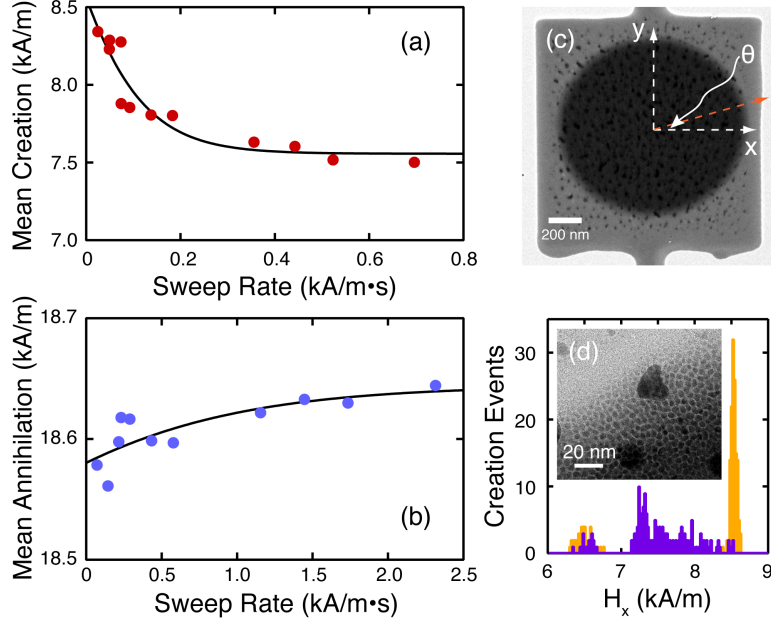


FIG. 4: Color online. (a) Mean creation and (b) annihilation fields versus sweep rate. Curves are guides to the eye. (c) TEM image of the magnetic disk on the resonator, with the direction of bias-field rotation. The dark flecks are the remnants of the gold on the opposite side of the nitride from the permalloy disk. (d) Rotation of the bias field can eliminate the supercooling with all else the same (sweep rate 0.36 kA/m·s): the dark (purple) histogram is 175 vortex creation events at 0 degrees and the light (orange) histogram is 175 events with the bias field rotated by 2 degrees. The inset shows a TEM micrograph of the ~ 5 nm crystalline grains at the edge of the disk. The large dark spots are the gold remnants.

rates. Rotation back to 0 degrees consistently recovers the supercooling effect. Moreover, the supercooling persists over angles between 0 and 2 degrees, and beyond 2 degrees, although the amount of supercooling is altered on the ~ 0.5 degree scale.

Two degrees corresponds to moving the vortex creation along the disk circumference by 17 nm, and 0.5 degrees by 4 nm. These numbers are consistent with the relevant length scales in the problem, which are the diameter of a vortex core, ~ 10 nm [2, 25], and the permalloy crystalline grain roughness, ~ 5 nm, as measured by transmission electron microscopy (TEM), inset to Fig. 4d. There are no large defects in the disk as can be seen in a TEM micrograph of the disk, Fig. 4c. It is by tuning the vortex entry position that we access the regime of sweep rate dependent supercooling on time scales that are experimentally obtainable. This has not been previously explored in single disk measurements [26]. LLG simulations of magnetic disks show that notches and bumps on the perimeter of a disk along the diameter perpendicular to the applied magnetic field direction

significantly affect the vortex creation field as compared to a smooth edge disk, which confirms the crucial role of edge roughness in nucleating a vortex.

In conclusion, we have observed a spreading and lowering of the vortex creation field in response to increasing magnetic field sweep rates. This originates from supercooling of the high-field to vortex-state transition, due to a barrier to forming a vortex with out of plane magnetization. This is experimental evidence that the transition to the vortex state in a single magnetic disk can be described in terms of a modified Landau first-order phase transition [11]. The vortex supercooling can be eliminated by small angle rotations of the applied bias field, which causes vortex creation and annihilation at a different position along the magnetic disk's perimeter with a different vortex nucleation barrier associated with different local regions of magnetic crystalline grains. These observations will affect possible use of magnetic nanodisks as information storage media because of the long time scale for vortex core nucleation [10]. Finally, we suggest that future measurements on magnetic disks with very low edge roughness and controlled localized defects for vortex creation and annihilation [27], will shed even more light on this subject.

This work was supported by NSERC, iCORE, CIFAR, NINT, CRC, AIF, and the Integrated Nanosystems Research Facility supported through CFI and nanoAlberta. We thank Don Mullin, Greg Popowich, Tony Walford and Steve Launspach for their contributions.

-
- [1] A.A. Thiele, *Phys. Rev. Lett.* **30**, 230 (1973).
 - [2] K.Yu. Guslienko and K.L. Metlov, *Phys. Rev. B* **63**, 100403(R) (2001).
 - [3] K.Yu. Guslienko, V. Novosad, Y. Otani, H. Shima and K. Fukamichi, *Phys. Rev. B* **65**, 024414 (2001).
 - [4] J. Bigot, M. Vomir and E. Beaurepaire, *Nature Phys.* **5**, 515 (2009).
 - [5] K. Yamada, S. Kasai, Y. Nakatani, K. Kobayashi, H. Kohno, A. Thiaville and T. Ono, *Nature Mat.*, **6**, 269 (2007).
 - [6] A.V. Kimel, B.A. Ivanov, R.V. Pisarev, P.A. Usachev, A. Kirilyuk and Th. Rasing, *Nature Phys.*, **5**, 727 (2007).
 - [7] C. La-O-Vorakiat, *et al.*, *Phys. Rev. Lett.* **103**, 257402 (2009).
 - [8] L. Néel, *Ann. Géophys.* **5**, 99 (1949).
 - [9] W.F. Brown, *Phys. Rev.* **130**, 1677 (1963).
 - [10] M.P. Sharrock, *IEEE Trans Magn.* **35**, 4414 (1999).

- [11] S. Savel'ev and F. Nori, Phys. Rev. B **70**, 214415 (2004).
- [12] S.D. Bader, Rev. Mod. Phys. **78**, 1 (2006).
- [13] R. Antos, Y.C. Otani and J. Shibata, J. Phys. Soc. Japan **77**, 031004 (2008).
- [14] L.D. Landau, E.M. Lifshitz and L.P. Pitaevskii, *Electrodynamics of Continuous Media 2nd Edition* (Pergamon Press, Oxford 1984).
- [15] K. Binder, Rep. Prog. Phys. **50**, 783 (1987).
- [16] P. Schiffer and D.D. Osheroff, Rev. Mod. Phys. **67**, 491 (1995).
- [17] J.P. Davis, D. Vick, D.C. Fortin, J.A.J. Burgess, W.K. Hiebert and M.R. Freeman, Appl. Phys. Lett. **96**, 072513 (2010).
- [18] Norcada, 4465 - 99 St. Edmonton, Alberta, Canada T6E 5B6.
- [19] M.M. Deshmukh, D.C. Ralph, M. Thomas and J. Silcox, Appl. Phys. Lett. **75**, 1631 (1999).
- [20] M. Rahm, *et al.*, Appl. Phys. Lett. **82**, 4110 (2003).
- [21] M. Schneider, H. Hoffmann and J. Zweck, Appl. Phys. Lett. **77**, 2909 (2000).
- [22] A. Garg, Phys. Rev. B **51**, 15592 (1995).
- [23] J.P. Park, P. Eames, D.M. Engebretson, J. Berezovsky and P.A. Crowell, Phys. Rev. Lett. **89**, 277201 (2002).
- [24] B.A. Ivanov and C.E. Zaspel, J. of Appl. Phys. **95**, 7444 (2004).
- [25] A. Wachowiak, J. Wiebe, M. Bode, O. Pietzsch, M. Morgenstern and R. Wiesendanger, Science **298**, 577 (2002).
- [26] G. Mihajlovic, *et al.*, Appl. Phys. Lett. **96**, 112501 (2010).
- [27] M.H. Park, Y.K. Hong, S.H. Gee, D.W. Erickson and B.C. Choi, Appl. Phys. Lett. **83**, 329 (2003).